Technology

Microelectronic Structures

Controlling contamination in Mo/Si multilayer mirrors by Si surface-capping modifications
Malinowski, M., C. Steinhaus, M. Clift, L.E. Klebanoff, S. Mrowka, R. Soufli

Determination of formal oxidation state of Co in MBE-grown co-doped TiO_2(001) anatase epitaxial films by x-ray absorption spectroscopy
Chambers, S.A., T. Droubay, S. Thevuthasan, N.H. Hamdan

High resolution study of the thermomechanical behavior of Al(0.5wt% Cu) thin films by scanning x-ray microdiffraction (μSXRD)
Tamura, N., B.C. Valek, R. Spolenak, R.S. Celestre, A.A. MacDowell, H.A. Padmore, B.W. Batterman, J.R. Patel

Infrared conductivity of photocarriers in organic molecular crystals
Weber, C., Ch. Kloc, M. Martin, J.H. Schoen, B. Batlogg, J. Orenstein

Macro stress mapping on thin film buckling
Goudeau, P., P. Villain, N. Tamura, R.S. Celestre, H. Padmore

Controlling Contamination in Mo/Si Multilayer Mirrors by Si Surface-capping Modifications

M. Malinowski[1], C. Steinhaus[1], M. Clift[1], L. E. Klebanoff [1], S. Mrowka[2], R. Soufli[3]
[1]Sandia National Laboratories, Livermore, CA 94551
[2]Lawrence Berkeley National Laboratory, Berkeley, CA 94720
[3]Lawrence Livermore National Laboratory, Livermore, CA 94551

INTRODUCTION

The present experiments helped determine the influence of the Si capping layer thickness in Mo/Si multilayer mirrors (MLMs) on the initial carbon (C) buildup on the mirrors when used in an extreme ultraviolet (EUV) + low pressure hydrocarbon (HC) vapor environment. The intent of this work was to broaden the approach taken to fabricate multilayer mirrors, by proposing that MLMs be made so that they have not only high initial reflectances but also low C buildup when used in EUV + HC environments. Carbon buildup is undesirable since it absorbs EUV radiation and reduces MLM reflectivity.

Previous work [1-4] on non-multilayer optical elements in synchrotron beamlines has shown that the "cracking" of hydrocarbons adsorbed on the optical surfaces leads to deposition of carbon onto these surfaces. "Cracking" is the name given to the process in which adsorbed, potentially volatile hydrocarbons are transformed into stable carbonaceous species on a surface. In these previous studies [2-4], it was determined that this cracking was caused by photoelectrons emitted from the metallic optical surfaces.

When EUV radiation is incident onto a MLM there is a sinusoidally varying, standing wave electric field both inside and outside the MLM structure. This incident photon radiation creates a standing wave, electric field intensity (and similarly modulated photoemission) with a period of half the wavelength of the incident EUV light. Since the cracking of adsorbed hydrocarbons is likely caused by photoelectrons [2-4], in principle the initial carbon contamination on MLM surfaces could be reduced by appropriately adjusting the electric field intensity at the uncontaminated MLM/vacuum interface so the field intensity is near a minimum.

One way to vary this intensity at the MLM/vacuum interface is through intentional changes in the thickness of the MLM Si capping layer. A set of Mo/Si MLMs deposited on Si wafers was fabricated such that each MLM had a different Si capping layer thickness ranging from 2 nm to 7 nm. Each was deposited such that maximum reflectance occurred at normal incidence for photons of 13.4 nm wavelength and had Mo/Si bilayer pairs about 6.9 nm thick, with Mo/(Mo+Si) thickness ratios of 0.4. These samples were used in subsequent EUV+HC tests.

RESULTS

It was found that the capping layer thickness affected both the initial MLM reflectivity and the "carbonizing" tendency on the MLM when exposed to EUV(13.4 nm, ~ 0.5 mW/mm^2) + HC vapors (pressures estimated to be $< 10^{-8}$ Torr). Measurements of the uncontaminated, absolute reflectivities were performed on the Calibration and Standards beamline at the ALS and are given in Figure 1 below. Figure 2 below shows the relative reflectivities (reflectivity/original reflectivity) for all samples which were subsequently exposed to EUV + HC vapors.

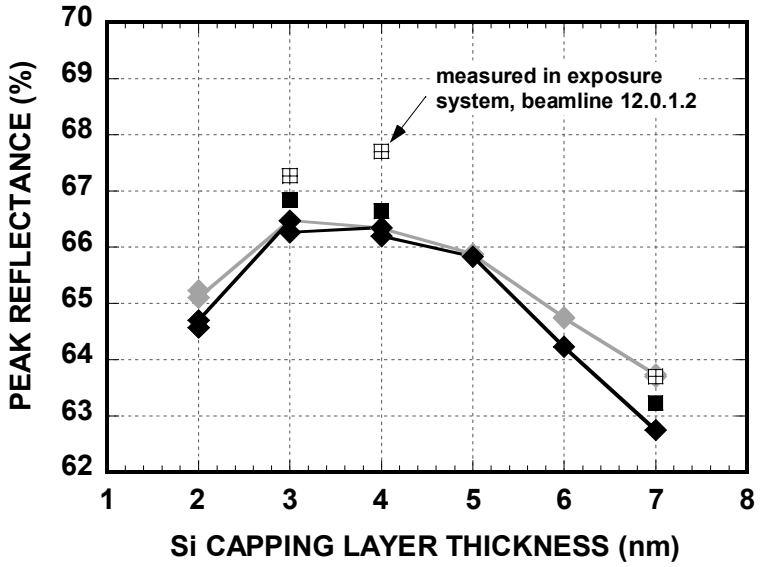

Figure 1. Absolute reflectances of all samples in used in this study. Reflectances were measured in regions not exposed to EUV+HC vapors. Values measured on beamline 12.0.1.2 are shown as squares with inset crosses. All other values were measured on beamline 6.3.2 before the experimental runs (gray points) and after experimental runs (black points).

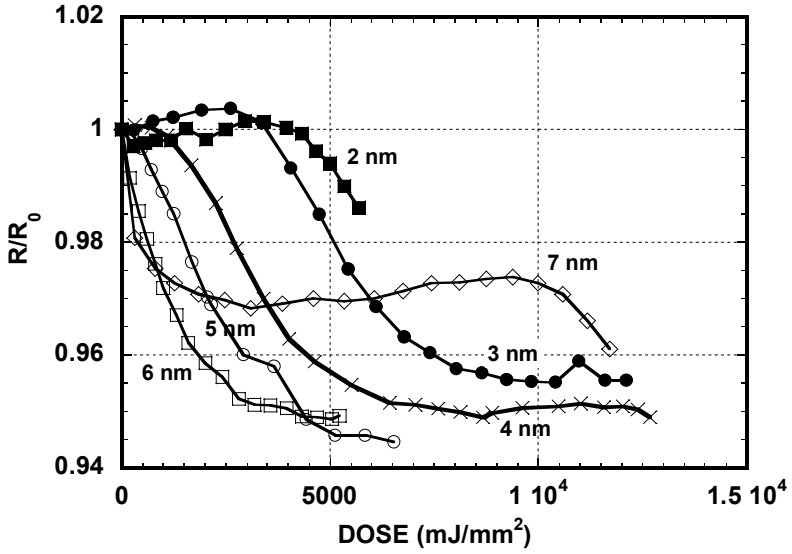

Figure 2. Relative reflectances) of samples with different capping layers exposed to EUV+HC as a function of photon dose.

In these samples, the doses where the relative reflectivities decreased most rapidly (e.g., at ~ 5000 mJ/mm^2 for the 3 nm capped sample) were also the doses where peaks in photocurrent emission occurred. These observations were consistent with the proposed correlation between photoemission (or near-surface electric field intensity) and carbon buildup. The results in both these figures also show that the use of a 3 nm capping layer on a Mo/Si MLM represents an improvement over the 4 nm layer since the 3 nm sample has both a higher absolute reflectivity and better initial resistance to carbon buildup. A typical Mo/Si MLM has a ~ 4.3 nm Si cap.

SUMMARY

The results of this work have shown that varying the silicon capping layer can change the characteristics of carbon buildup on a Mo/Si MLM optic. The data obtained indicated that a ~3 nm Si- capped Mo/Si MLM was the MLM which not only had the highest as-received reflectivity but also maintained that reflectivity the longest under EUV+HC vapor pressure exposure of the samples studied – those with Si capping layers from 2 nm to 7 nm. Using a 3 nm instead of 4 nm thick Si capping layer on Mo/Si MLMs should produce improved optic lifetimes and should likewise help reduce downtimes in EUVL tools using such optics. This work also showed that there is a strong correlation between the EUV-induced photocurrent from a MLM and its reflectivity, with maxima in the photocurrents occurring when relative reflectivity loss rates were the highest. This observation suggested that the carbon buildup was also correlated with photoemission, with higher carbon growth rates coincident with higher MLM photoemission. However, since the maxima in surface electric fields at the MLM are correlated with photoemission maxima, the current data did not allow a differentiation between the mechanisms of direct photon vs. photoelectron-caused hydrocarbon cracking. The current data were consistent with the existence of a standing wave electric field near the MLM surface and suggest that its form profoundly affected carbon contamination of MLMs. The results further suggested that the strategy of minimizing the near- surface electric field at the MLM/vacuum to reduce carbon buildup should be applicable to MLM systems other than conventional Mo/Si, including Mo/Si with other capping layers and MLMs using other material combinations

ACKNLOWLEDGMENTS

The beamline assistance and advice of Ken Goldberg, Patrick Naulleau, Paul Denham, Frank Zucca of LBNL were critical to our work. The expert technical assistance of Fred Grabner of LLNL in fabricating all mutltilayers is acknowledged. We are grateful to Ben Kaufmann and Andy Aquila of LBNL for performing the multilayer reflectivity measurements.

REFERENCES

[1] D.A. Shirley, "Beam Line Chemistry," in Workshop on X-Ray Instrumentation for Synchrotron Radiation Research (H. Winick and G. Brown, eds.), SSRL Report no. 78/04 (May, 1978), VII-80.

[2] K. Boller, R.-P. Haelbich, H. Hogrefe, W. Jark and C. Kunz, *Nucl. Instrum. And Meth.* **208** (1983) 273.

[3] R. A.Rosenberg and D. C. Mancini, Nucl. Instrum. And Meth. In Physics Research **A291** (1990) 101.

[4] T. Koide, S. Sata, T. Shidara, M. Niwano, M. Yanagihara, A. Yamada, A. Fujimori, A. Mikuni, H. Kato, and T. Miyahara, Nucl. Instrum. And Meth.. in Physics Research **A246** (1986) 215.

This work was supported by the Extreme Ultraviolet Limited Liability Company (EUV LLC) and by the U. S. Department of Energy under Contract DE-AC04-94L85000.

Principal investigator: Michael E. Malinowski, Sandia National Labororatories. Email: memalin@sandia.gov. Telephone: 925-294-2069

Determination of Formal Oxidation State of Co in MBE-Grown Co-doped TiO_2(001) Anatase Epitaxial Films by X-ray Absorption Spectroscopy

S.A. Chambers[1], T. Droubay[1], S. Thevuthasan[1], N.H. Hamdan[2]
[1]Fundamental Science Division, Pacific Northwest National Laboratory
Richland, WA 99352, U.S.A.
[2]Lawrence Berkeley National Laboratory, Berkeley, CA 94720, U.S.A.

INTRODUCTION

Diluted magnetic semiconductors (DMS) consist of nonmagnetic semiconducting materials doped with a few atomic percent of impurity magnetic cations. Magnetic coupling occurs by virtue of exchange interactions between the magnetic spins and free carriers in the semiconductor. The interaction can occur via *p-d* or *d-d* exchange, and can lead to antiferromagnetic or ferromagnetic coupling, depending on the concentration and the local structural environment of the magnetic impurity. DMS materials grown as thin epitaxial films can be used as spin injectors for semiconductor heterostructures, provided they are ferromagnetic.

Virtually all conventional DMS materials exhibit Curie temperatures of ~100K or less and must be *p*-type, which means that the exchange interaction leading to ferromagnetic behavior is hole mediated. Most of the effort expended to date on understanding the crystal growth and properties of thin-film DMS materials has focused on Mn-doped II-VI, III-V, and Group IV semiconductors.[1-4] Relatively little effort has gone into the investigation of "nontraditional" semiconductors, such as semiconducting oxides, to see if they are more robust magnetically. However, one such oxide - Co-doped TiO_2 anatase ($Co_xTi_{1-x}O_2$) - has recently been discovered to be the most magnetically robust DMS with regard to magnetic moment at saturation, coercivity, remanence, and Curie temperature.[5] Indeed, it is one of the very few DMS materials demonstrated to exhibit ferromagnetic behavior above 300K. In addition, it has been shown that the material can be grown epitaxially by both pulsed laser deposition (PLD)[6] and oxygen plasma assisted molecular beam epitaxy (OPA-MBE)[5] on $SrTiO_3$(001) and $LaAlO_3$(001). However, the resulting magnetic properties differed considerably for the two growth methods, with significantly better properties exhibited by OPA-MBE grown material.

In order to understand the mechanism of magnetism in this fascinating material, it is essential to know the charge state of the magnetic cation (Co), and the doping type. We have utilized Co L-edge x-ray absorption spectroscopy (XAS) at beamline 9.3.2 to determine the Co charge state.

EXPERIMENT

Epitaxial $Co_xTi_{1-x}O_{2-x}$ films of high structural quality were grown by OPA-MBE on $LaAlO_3$(001)[7] using a system at PNNL described in detail elsewhere.[8] The resulting samples were then transferred through air to beamline 9.3.2 and XAS measurements were made in total electron yield mode at the Co L-edge, Ti L-edge, and O K-edge. X-ray absorption near-edge spectra (XANES) were also recorded for several Co standards for comparison purposes. No surface cleaning was done, as the distribution of Co has been shown to be strongly modified by post-growth annealing at the temperatures required to rid the surface of carbon, or remove sputter damage.

RESULTS

We show in Fig. 1 Co L-edge XAS data for three films with different Co mole fractions (x) (Fig. 1a-c), and for standards containing Co in different oxidation states and local structural environments (Fig. 1d-g). The $CoTiO_3$ standard was a powder, CoO was a (001)-oriented bulk single crystal, γ-Co_2O_3 was a 100 nm thick (001)-oriented epitaxial film grown on MgO(001) at PNNL, and the Co metal standard was a polycrystalline film evaporated *in situ* in the XAS chamber. Comparison of all film spectra with those for the standards reveals a good fit with both $CoTiO_3$ and CoO, which both contain Co^{+2}, but a very poor fit for both γ-Co_2O_3, which contains Co^{+3}, and for Co metal. The fit to $CoTiO_3$ is better than that to CoO. However, there is some similarity between the reference spectra for CoO and γ-Co_2O_3, particularly in the vicinity of the feature at 784 eV. This result indicates that there may be some Co^{+3} in the CoO single crystal. The very high degree of similarity between the spectra for the Co-doped anatase films and the $CoTiO_3$ standard establishes that Co in the former is in the +2 formal oxidation state. Interestingly, using the Co evaporation rate and oxygen plasma beam intensity we have used for the growth of $Co_xTi_{1-x}O_{2-x}$ result in the epitaxial growth of metastable γ-Co_2O_3 on MgO(001). Therefore, the anatase lattice stabilizes the formation of Co(II), even though the conditions would result in Co(III) formation if pure Co oxide were allowed to grow under comparable

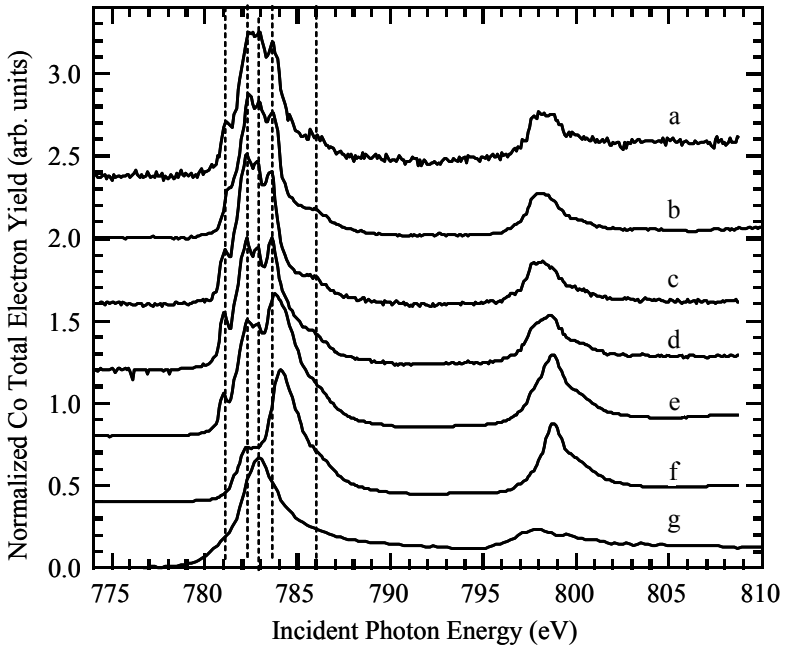

conditions.

Fig. 1 Co L-edge XAS for 20 nm thick films of epitaxial $Co_xTi_{1-x}O_{2-x}$ on $LaAlO_3$(001): (a) x = 0.01, (b) x = 0.06, (c) x = 0.08. Also shown are spectra for reference compounds containing Co in different formal oxidation states: (d) $CoTiO_3$, (e) CoO, (f) γ-Co_2O_3, and (g) Co metal.

SIGNIFICANCE

Ion channeling measurements conducted at PNNL reveals that Co substitutes for Ti in the anatase lattice. Furthermore, Hall effect measurements carried out at PNNL show that these films are *n*-type semiconductors as grown, despite the fact that no intentional *n*-type doping was carried out. The origin of the *n*-type doping may have to do with the presence of H in the film,

which has been detected by ^{19}F nuclear reaction analysis at PNNL at a concentration that is of the same order of magnitude as that of the free carriers – 10^{19} to 10^{20} cm^{-3}. H may be the direct dopant, as occurs in *n*-ZnO.[9] Alternatively, H_2, which is present in the growth chamber at a very low partial pressure, may partially reduce lattice oxygen during growth to produce OH and a free donor electron according to the reaction $O^{-2}_{(lattice)} + (1/2)H_2 \rightarrow OH^-_{(lattice)} + e^-$. This phenomenon is currently under more detailed investigation.

It thus appears that Co-doped anatase TiO_2 is ferromagnetic by virtue of *electron* mediated exchange interaction between Co^{+2} cations that substitute for Ti^{+4} in the lattice. In order to maintain charge neutrality, each substitutional Co^{+2} must be accompanied by an O^{-2} vacancy. However, such vacancies are uncharged and therefore do not contribute any donor electrons. In fact, *n*-type semiconducting behavior and Co substitution are independent phenomena; some highly resistive films are nonmagnetic despite having several at. % Co. Indeed, the magnetization depends as much on the free carrier concentration as on the presence of substitutional Co, as expected for a DMS.

Significantly, virtually all other known DMS materials are ferromagnetic by virtue of *hole* mediated exchange interaction, which has been thought to be the stronger interaction.[10] Therefore, Co-doped TiO_2 anatase is a highly unusual and potentially very important DMS in that it exhibits strong electron mediated exchange interaction at temperatures of at least 500K. No other known DMS exhibits these properties.

REFERENCES

1. R. Fiederling, M. Keim, G. Reuscher, W. Ossau, G. Schmidt, A. Waag, L.W. Molenkamp, Nature **402**, 787 (1999).
2. B.T. Jonker, Y.D. Park, B.R. Bennett, H.D. Cheong, G. Kioseoglou, A. Petrou, Phys. Rev. **B62**, 8180 (2000).
3. R.K. Kawakami, Y. Kato, M. Hanson, I. Malajovich, J.M. Stephens, E. Johnston-Halperin, G. Salis, A.C. Gossard, D.D. Awschalom, Science **294**, 131 (2001).
4. Y.D. Park, A.T. Hanbicki, S.C. Irwin, C.S. Hellberg, J.M. Sullivan, J.E. Mattson, T.F. Ambrose, A. Wilson, G. Spanos, B.T. Jonker, Science **295**, 651 (2002).
5. S.A. Chambers, S. Thevuthasan, R.F.C. Farrow, R.F. Marks, J.-U. Thiele, L. Folks, M.G. Samant, A.J. Kellock, N. Ruzycki, D.L. Ederer, U. Diebold, Appl. Phys. Lett. **79**, 3467 (2001), and, S.A. Chambers, Mat. Today, to appear, April issue (2002).
6. Y. Matsumoto, M. Murakami, T. Shono, T. Hasegawa, T. Fukumura, M. Kawasaki, P, Ahmet, T. Chikyow, S.-Y. Koshihara, H. Koinuma, Science **291**, 854 (2001).
7. S.A. Chambers, C. Wang, S. Thevuthasan, T. Droubay, D.E. McCready, A.S. Lea, V. Shutthanandan, C.F. Windisch, Jr., submitted to Thin Solid Films (2002).
8. S.A. Chambers, Surf. Sci. Rep. **39**, 105 (2000).
9. D.M. Hofman, A. Hofstaetter, F. Lieter, H. Zhou, F. Henecker, B.K. Meyer, S.B. Orlinskii, J. Schmidt, and P.G. Baranov, Phys. Rev. Lett. **88**, 045504-1 (2002).
10. T. Dietl, H. Ohno, F. Matsukura, J. Cibert and D. Ferrand, Science **287**, 1019 (2000).

The work was funded by a Laboratory Directed Research and Development grant associated with the PNNL Nanoscience and Technology Initiative, and by DOE BES Materials Science.

Principal Investigator – S.A. Chambers. Phone – (509) 376-1766. E-mail – sa.chambers@pnl.gov

High Resolution Study of the Thermomechanical Behavior of Al(0.5wt% Cu) Thin Films by Scanning X-Ray Microdiffraction (μSXRD)

N. Tamura[1], B.C. Valek[3], R. Spolenak[2], R.S. Celestre[1], A.A. MacDowell[1], H.A. Padmore[1], B.W. Batterman[1,4] and J.R. Patel[1,4]

[1]Advanced Light Source, Ernest Orlando Lawrence Berkeley National Laboratory, University of California, Berkeley, California 94720, USA

[2]Agere Systems, formerly Bell Laboratories, Lucent Technologies, Murray Hill NJ 07974

[3]Dept. Materials Science & Engineering, Stanford University, Stanford CA 94305

[4]SSRL/SLAC, Stanford University, P.O. Box 43459, Stanford CA 94309, USA

INTRODUCTION

Materials properties such as strength, resistance to fatigue, and failure ultimately depend on the microstructural features of the material, such as grains, grain boundaries, inclusions, voids and other defects. The so-called mesoscopic length scale (approximately between 0.1 and 10 μm) is receiving increasing attention, both theoretically and experimentally, in order to understand the mechanical behavior of polycrystalline samples as they experienced various constraints. Compared to single crystals, polycrystals are a highly inhomogeneous medium where local stress and structure variations are likely to play an important role in the overall macroscopic behavior of the material. In the present study, we are applying the Scanning X-Ray Microdiffraction (μSXRD) technique developed at the ALS [1,2] to probe local strain/stress and grain orientation in Al(0.5wt% Cu) thin films and compare the results with those obtained with conventional averaging techniques such as wafer curvature.

EXPERIMENTAL

The samples investigated are sputtered Al (0.5 wt.% Cu) thin film test structures originally designed for electromigration studies. The patterned lines, passivated with 0.7 μm of SiO_2 (PETEOS), have dimensions 0.7 or 4.1 μm in width, 30 μm in length and 0.75 μm in thickness. Ti shunt layers are present at the bottom and the top of the lines. A 100 x 100 μm bond pad on the chip with a thin Ti underlayer is used to simulate a bare blanket film.

The samples were scanned under a submicron size white X-ray beam and at each step a white beam Laue diffraction pattern in reflective geometry was collected. The patterns were analyzed in order to yield the orientation and deviatoric strain/stress tensor under each illuminated points of the samples. The outputs of the analysis are grain orientation and strain/stress maps.

The bond pad (blanket film) was thermally cycled between 25°C and 345°C in 40° steps. At each temperature increment, a 15x15 μm area of the film was scanned with the focused white x-ray beam in 1 μm steps. A 0.7 μm wide line and 4.1 μm wide line were scanned in 0.5 μm intervals at room temperature. In addition, a 0.7 μm line was mapped in 0.5 μm steps across the line and 1 μm steps along the line at several temperatures during a cycle between 25°C and 305°C.

RESULTS

A 5x5 μm area preliminary scan of the blanket film shows that while the film is (111) textured within 3°, the deviatoric stresses $\sigma_{xx}' \neq \sigma_{yy}'$ (In the x,y,z orthogonal coordinate system, z is the

out-of-plane direction). In particular, at the granular and subgranular level, the stress can depart significantly from biaxiality. However, if we average the data over the 5 × 5 μm scanned area, biaxiality is retrieved, i.e.: $\langle\sigma'_{xx}\rangle \approx \langle\sigma'_{yy}\rangle$. The average biaxial stress of the film can be computed assuming that the out-of-plane average total stress $\langle\sigma_{zz}\rangle = 0$. Expressing the total average stress matrix as the sum of the deviatoric and hydrostatic stress components one can show that the average biaxial stress $\langle\sigma_b\rangle = \langle\sigma_{xx}\rangle = \langle\sigma_{yy}\rangle = \langle\{(\sigma'_{xx}+\sigma'_{yy})/2\} - \sigma'_{zz}\rangle$.

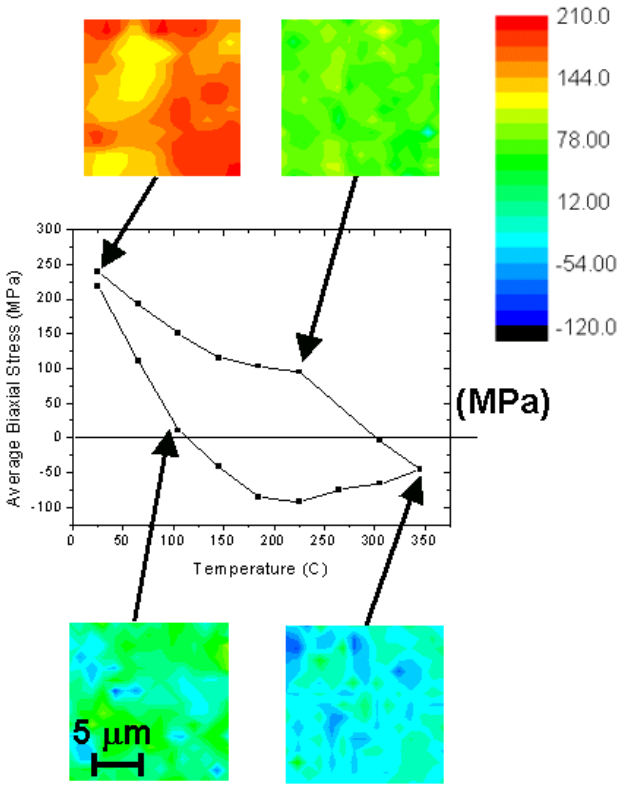

Figure 1. Thermal cycling results on a 15×15 μm area of an Al(Cu) bond pad (blanket film) showing the averaged biaxial stress component $\langle\sigma_b\rangle$ versus temperature. The insets show detailed stress distribution in the film at different temperatures (The 2D maps are a plot of $-\sigma'_{zz} = \sigma'_{xx} + \sigma'_{yy}$ as a measure of the in-plane stress). Note the blue regions of compressive stress in the 105 ºC map, while on average the stress is still in the tensile regime.

A plot of the average biaxial stress in the blanket film obtained by x-ray microdiffraction during a thermal cycle between 25°C and 345°C is shown in Fig. 1. The stresses in approximately 130 grains in a 15μm x 15μm region were averaged to give the results shown in the figure. Though our temperature range is about 100°C smaller, the temperature cycling curve using microdiffraction is very similar to that reported by Venkatraman et al [3] using wafer curvature measurements on an Al(Cu) films with thickness 1 μm. The film is in tension at room temperature, with an average biaxial stress of 230 MPa. The measured stress is caused by mismatch between the thermal expansion coefficients of the aluminum and the silicon substrate. Upon heating, the higher thermal expansion coefficient of the aluminum film relaxes the tensile stress before driving the film into compression. From Fig. 1 the experimentally determined initial thermoelastic slope is $(d\sigma / dT) = 2.53$ MPa / °C. The theoretical thermoelastic slope was calculated to be 2.34 MPa / °C, in reasonable agreement with the experimental value.

The real advantage of using μSXRD is however the possibility to obtain orientation and strain/stress information at a very local level, allowing for the study of mechanical properties of thin films with new visibilities. For instance, it provides a simple and straightforward explanation to the early departure from linearity of the thermoelastic slope during heating (seen in [3] as well as in the present data), even before the film enters in the compressive state. At room temperature, the stress is highly inhomogeneous with regions sustaining more tensile stress than others. Upon

heating some regions of the film become compressive while the average biaxial stress is still in the tensile regime. Even though the average stress is zero at about 100^{o}C some grains have already reached their yield stress and deformed and the heating curve departs from linearity. The temperature at which the curve departs from linearity is quite variable for different films and depends on detailed process parameters.
Similar local variations of the stress are observed in the passivated lines. These local variations increase with decreasing line width while the area of the hysterisis of the stress-temperature curves decreased. The hysteresis area is typically a measure of the amount of plastic deformation experienced by the material. In the case of submicron sized lines, the passivation layers introduce additional constraints to the dislocation motions, as compared to the case of unpassivated blanket films [4]. These local stress variations which do not always follow grain boundaries but can be intragranular, are quite surprising in an elastically isotropic material as aluminum. However these differences can be explained by differences in grain sizes and grain-to-grain interactions [5].

ACKNOWLEDGMENTS

The authors thank Intel Corp. for the partial funding of the end station.

REFERENCES

1. A. A. MacDowell, R. S. Celestre, N. Tamura, R. Spolenak, B. Valek, W. L. Brown, J. C. Bravman, H. A. Padmore, B. W. Batterman, and J. R. Patel, Nucl. Instr. & Meth. In Phys. Res. **A 467-468**, 936 (2001).
2. N. Tamura, R. Spolenak, B.C. Valek, A. Manceau, N. Meier Chang, R.S. Celestre, A.A. MacDowell, H.A. Padmore and J.R. Patel, Rev. of Sci. Instr., **73** (2002) in press.
3. R. Venkatraman, J. C. Bravman, W. D. Nix, P. W. Davies, P. A. Flinn, D. B. Fraser. J. of Electron. Matls. **19**, 1231 (1990).
4. B.C. Valek, N. Tamura, R. Spolenak, A.A. MacDowell, R.S. Celestre, H.A. Padmore, J.C. Bravman, W.L. Brown, B. W. Batterman and J. R. Patel, Mat. Res. Soc. Symp. Proc., **673**, P.7.7.1 (2001).
5. R. Spolenak et al. (2002) this compendium.

This work was supported by the Director, Office of Science, Office of Basic Energy Sciences, Materials Sciences Division, of the US Department of Energy under Contract No. DE-AC03-76SF00098 at Lawrence Berkeley National Laboratory.

Principal investigator: Nobumichi Tamura, Advanced Light Source, Ernest Orlando Lawrence Berkeley National Laboratory. Email: NTamura@lbl.gov. Telephone: 510-486-6189.

Infrared conductivity of photocarriers in organic molecular crystals

Chris Weber*[1,2], Ch. Kloc[3], Michael Martin[4], J.H. Schoen[3], B. Batlogg[3], Joe Orenstein[1,2]
[1] Department of Physics, University of California, Berkeley, CA 94720
[2] Material Sciences Division, Lawrence Berkeley National Laboratory, Berkeley, CA 94720
[3] Bell Laboratories, Lucent Technologies, Murray Hill, New Jersey 07974-0636
[4] Advanced Light Source Division, Lawrence Berkeley National Laboratory, Berkeley, CA 94720

This project, begun in March of 2001, seeks use infrared spectroscopy to probe the properties of photocarriers in organic molecular crystals. A group at Bell Laboratories has recently succeeded in creating FETs on ultrapure single crystals of pentacene, tetracene, and other "polyacenes" (rigid, rodlike chains of Benzene rings). Carriers injected into these transistors have exhibited metal-insulator transitions, superconductivity, lasing, and the quantum Hall effect (see, e.g., J. H. Schoen, Ch. Kloc, B. Batlogg, *Science* v. 288 p. 2338; *Science* v. 288 p. 656; *Nature* v. 406 p. 702). The goal of our experiment is to photoexcite carriers in these same materials, and to measure the infrared spectrum of these photocarriers.

The apparatus, at ALS beamline 1.4, includes an Argon-ion laser for photoexcitation of charge carriers, a Bruker 66v/S Fourrier-Transform Infrared (FTIR) spectrometer, and a variable-temperature cryostat. The laser allows photoexcitation at energies from 2.4 eV to 3.5 eV. At the UV frequencies, the quantum efficiency of photocarrier generation in pentacene is high, about 30%. The light is coupled to the sample (in the cryostat) by means of an optical fiber. The cryostat allows us to reach temperatures from 5 K to 300 K, and the FTIR spectrometer allows measurement of infrared transmission on the range of at least 100 cm^{-1} to 7800 cm^{-1}.

The basic result of a measurement is a transmission spectrum, $T(\omega)$, either with the sample illuminated with laser light, $T_{on}(\omega)$, or with the sample unilluminared, $T_{off}(\omega)$. From these spectra we determine difference spectra, $\Delta T / T = (T_{on}(\omega) - T_{off}(\omega)) / T_{off}(\omega)$. Our measurements at room temperature on crystals of Tetracene have shown good reproducibility, both in the shape and in the magnitude of the difference spectra. The measurement is sensitive to changes in the transmission of one part in 10^4 or better through most of the spectral range. We have resolved many clear and reproducible features that are an order of magnitude larger than the noise.

Although these results demonstrate that the apparatus is, indeed, able to make the desired measurements, they do not put us particularly close to our scientific goals. Most or all of the features we have seen thus far appear to be due to shifting or broadening of phonon absorptions due to the heating effect of the laser. This result at room temperature is no surprise, as the mobility of carriers in polyacene crystals increases as T^{-2} below room temperature, so that the conduction of the carriers should only become visible at low temperatures. More surprising was the result that tetracene crystals large enough to measure optically will invariably shatter upon cooling below about 180 K (the temperature seems to vary a bit). Pentacene crystals, on the other hand, do not shatter, but also do not seem to be available in sizes large enough for optical measurement. Other

polyacenes have much lower efficiencies of photocarrier generation (due to their having broader bandgaps), and so are not suited to this experiment.

We are now seeking thin-film samples of the polyacenes, as these should survive cooling and should have the large area desirable for infrared measurement. High-quality pentacene films have been shown to display many of the same electronic properties as their single-crystal counterparts (J. H. Schoen, Ch. Kloc, *Applied Physics Letters*, v. 79, p. 4043).

Funding sources: This work and the Advanced Light Source are supported by the Director, Office of Science, Office of Basic Energy Science, Material Science Division, of the United States Department of Energy under contract number DE-AC03-76SF00098 at Lawrence Berkeley National Laboratory.

* To whom correspondence should be addressed:
cpweber@lbl.gov
(510) 486-5879

MACRO STRESS MAPPING ON THIN FILM BUCKLING

P. Goudeau[1], P. Villain[1], N. Tamura[2], R.S. Celestre[2] and H. Padmore[2]
[1]Laboratoire de Métallurgie Physique, UMR 6630 CNRS, Université de Poitiers, SP2MI, Téléport 2, Bd M. et P. Curie, BP 30179, 86962 Futuroscope Chasseneuil cedex, FRANCE
[2]Advanced Light Source, LBNL, 1 Cyclotron Road, MS 2-400, Berkeley, CA, 94270, USA

INTRODUCTION

Thin films deposited by Physical Vapor Deposition techniques on substrates generally exhibit large residual stresses which may be responsible of spontaneous detachment of the film from the substrate (stress relaxation) and in the case of compressive stresses, thin film buckling. Although these effects are undesirable for future applications, one may take benefit of it for thin film mechanical properties investigation [1-4]. Since the 80's, a lot of theoretical works have been done to develop mechanical models and calculations (elasticity of thin plates, fracture mechanic) with the aim to get a better understanding of driven mechanisms giving rise to this phenomenon and thus to propose solutions to avoid such problems. Nevertheless, only a few experimental works have been done on this subject to support these theoretical results and nothing concerning local stress/strain measurement mainly because of the small dimension of the buckling (fig. 1). In this experiment, we propose to use micro beam x-ray diffraction available on synchrotron radiation sources as a local probe (spatial) for stress/strain analysis of thin film buckling. The main objectives are to apply x-ray micro beam diffraction in first for determining macro residual stresses at the top of the buckle (comparison with adherent region on the film) in different systems (W, Mo, Au on silicon) and in a second step for scanning the buckling with the smallest x-ray beam size in order to realize macro stress mapping.

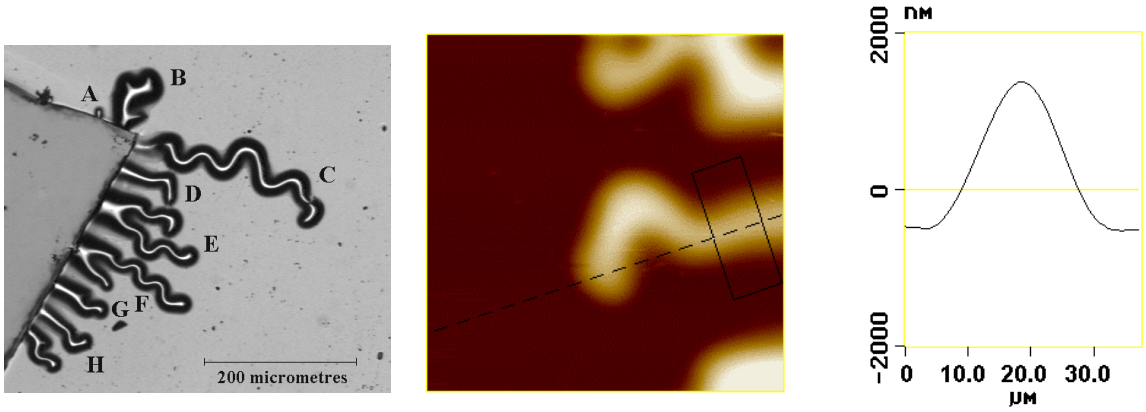

(a) (b) (c)

Figure 1 : *Wrinkles observed by optical microscopy (a) close to a step realised during the deposition process for film thickness measurement and AFM images (b) of buckling noted D on (a) and corresponding cross section, (c) perpendicular to the propagation direction.*

EXPERIMENTAL METHOD

Among the most widely used method to determine the stress level in thin films, x-ray diffraction (XRD) is phase selective and the unique non destructive technique which allows to determine both the mechanical and microstructural state of the diffracting phases. Indeed, the distance between atomic planes is used as an internal strain gauge. For polycrystalline samples, the

measurement of the diffraction peak position shift using $\sin^2\psi$ method allows to extract the stress tensor and the stress free lattice parameter [5]. However, x-ray diffraction is difficult to use in low dimensional systems because the diffracted intensities are weak due to the reduced thicknesses and nanocrystalline character of such materials. These problems may be solved using intense x-ray sources such as synchrotron radiation (S.R.). In addition to the high flux characteristic of S.R. facilities, the wide wavelength spectra and the optics (micro beam) which are available on beam lines (3^{rd} generation SR only) allow to perform specific XRD experiments which are not possible with classical x-ray sources in laboratories.

The 7.3.3.1 Microdiffraction beam line at ALS provides a reduced spot size less than 1 μm^2 (Kirkpatrick Baez mirrors) with high flux for white or monochromatic radiation (4-crystals channel cut monochromator: 6-14 KeV). These performances are unique and perfectly adapted to our project [6]. In our samples, the grain size ($\leq$ 10 nm) is smaller than the x-ray beam one and macro-strains are of about 0.5-1 %. The diffraction pattern recorded with a 2D CCD detector is composed of different rings which allow to extract (using specific software - to be developed) the in-plane stress without any tilt of the samples (the ψ *description* is contained in the 2D pattern and the angular resolution is enough to appreciate such large macro-strains). Accurate spatial spot localization on the sample surface is achieved from markers delimiting the region of interest. A precise goniometer allows XRD measurements in reflection mode and an X-Y translation stage is used for scanning the sample surface.

FEASIBILITY OF THE EXPERIMENT

Preliminary microdiffraction experiments have been successfully done in June 2001. 630 nm thick gold films deposited on silicon (100) substrates covered with native oxide have been chosen for these measurements. The delamination of the thin film is evidenced on figure 2 (a) and an individual buckle is shown on figure 2 (b); its shape corresponds to a portion of a sphere. The position of the buckle (x,y) is determined from the step corner coordinates (x0,y0) which have been measured by X-ray fluorescence (white beam). This step has been realized during the film deposition.

The calibration of the 2D diffraction diagram is done from the diffraction of the single crystal silicon substrate using white x-ray beam. The diffraction pattern obtained in an adherent (flat) region of the gold film is shown on figure 3. Because of the <111> texture of the film, we observe maximum intensities on each two rings for particular pole directions X. During the scan of the buckle A with a 10 μm step , the position of the two maximum intensities (X+ and X-) moves along the ring because of the rotation of the normal to the film surface around x and y axis. Thus, from the diffraction pattern, one may deduce the position of the beam on the buckle and the corresponding strains in this region. A comparison between the diffraction diagrams obtained in flat regions and at the top of the buckle indicates a stress relaxation.

A complete interpretation of the data is still under progress because specific tools and methodologies have to be applied for diffraction pattern analysis. Accuracy and sensibility are the two main points to be considered for strain variation during the scan. Furthermore, Finite Element calculations have been engaged for such spherical gold buckles. Further experiments will concern not only metallic thin films but also structural biomaterials such as diamond coatings on Titanium based alloys (TA6V) which are promising candidates for medical

prostheses. Our laboratory is engaged in a French government program called A.C.I. with two other French laboratories. It concerns in particular, the influence of residual stresses (about –5 GPa in C-diam) on the mechanical behavior of such systems.

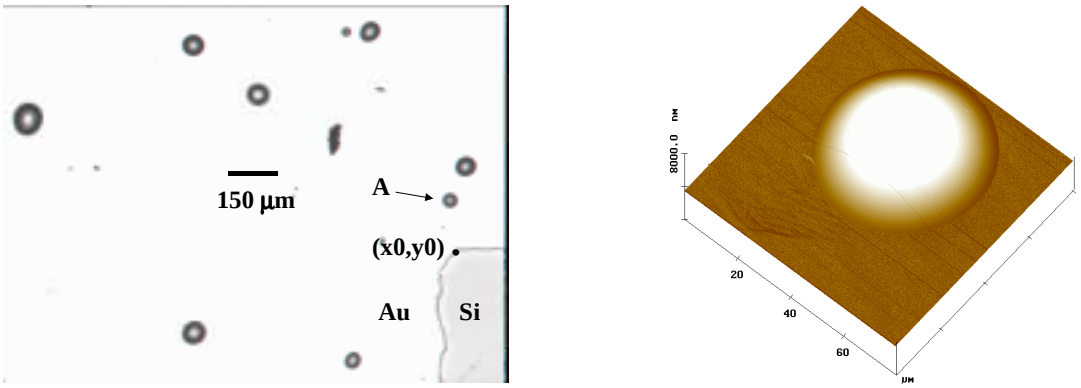

(a) (b)

Figure 2. *630 nm gold film sputter deposited on Si substrate: (a) optical image of the sample surface and (b) AFM image of the buckle noted A on fig. (a); the in plane width is around 40 µm and the height of 1.2 µm.*

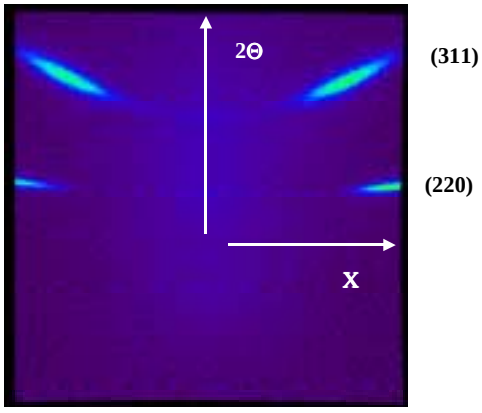

Figure 3: *2D X-ray diffraction diagram obtained on an adherent gold film region with an X-ray energy of 5.7 keV, a spot size on the sample of 3 x 3 µm^2 and a recording time of 300 sec.*

REFERENCES

1. M. Talea, B. Boubeker, F. Cleymand, C. Coupeau, J. Grilhé, P. Goudeau, Mat. Let. **41**, 181 (1999).
2. C. Coupeau, J.-F. Naud, F. Cleymand, P. Goudeau, J. Grilhé, Thin. Sol. Films **353**, 194 (1999).
3. V. Branger, C. Coupeau, P. Goudeau, B. Boubeker, K.F. Badawi, J. Grilhé, J. of Mat. Sci. Let. **19**, 353 (2000).
4. B. Boubeker, M. Talea, Ph. Goudeau, C. Coupeau, J. Grilhé, Mat. Charac. **45**, 33-37 (2000).
5. V. Branger, V. Pelosin, P. Goudeau, K.F. Badawi, High Temp. Mat. Proc. **2**, 419-429 (1998).
6. P. Goudeau in *Photomechanics 2001*, edited by Y. Berthaud et al.(GAMAC, France), 87-94.

This work was initiated with support of the Advanced Light Source at the Lawrence Berkeley National Laboratory.

Principal investigator: Philippe Goudeau, Laboratoire de Métallurgie Physique – UMR 6630 CNRS – Université de Poitiers, France. Email : Philippe.Goudeau@univ-poitiers.fr. Telephone : 33 5 49 49 67 26. Fax : 33 5 49 49 66 92